Phosphorylation regulates connexin43/ZO-1 binding and release, an important step in gap junction turnover

Anastasia F. Thévenin†, Rachel A. Margraf, Charles G. Fisher, Rachael M. Kells-Andrews, and Matthias M. Falk*
Department of Biological Sciences, Lehigh University, Bethlehem, PA 18015

ABSTRACT To investigate whether connexin phosphorylation regulates the known role of zonula occludens-1 protein (ZO-1) in gap junction (GJ) function, we generated and analyzed a series of phosphomimetic and phosphorylation-dead mutants by mutating known conserved regulatory serine (S) residues 255, 279/282, 365, 368, and 373 located in the C-terminal domain of connexin43 (Cx43) into glutamic acid (E) or alanine (A) residues. All connexin mutants were translated into stable, full-length proteins and assembled into GJs when expressed in HeLa or Madin–Darby canine kidney epithelial cells. However, mutants with S residues exchanged at positions 365, 368, and 373 exhibited a significantly altered ZO-1 interaction profile, while mutants with S residues exchanged at 255 and 279/282 did not. Unlike wild-type Cx43, in which ZO-1 binding is restricted to the periphery of GJ plaques, S365A, S365E, S368A, S368E, and S373A mutants bound ZO-1 throughout the GJ plaques, while the S373E mutant did not bind ZO-1 at all. Inability to disengage from ZO-1 correlated with increased GJ plaque size and increased connexin protein half-life, while maintaining GJ channels in an open, functional state. Quantitative clathrin-binding analyses revealed no significant alterations in clathrin-binding efficiency, suggesting that the inability to disengage from ZO-1 prevented maturation of functional into nonfunctional/endocytic channels, rather than ZO-1 interfering with GJ endocytosis directly. Collectively, our results indicate that ZO-1 binding regulates channel accrual, while disengagement from ZO-1 is critical for GJ channel closure and transitioning GJ channels for endocytosis. Intriguingly, these transitional ZO-1 binding/release and channel-aging steps are mediated by a series of hierarchical phosphorylation/dephosphorylation events at S373, S365, and S368, well-known Cx43 Akt, protein kinase A, and protein kinase C phosphorylation sites located in the vicinity of the ZO-1 binding site.

Monitoring Editor
Alpha Yap
University of Queensland

Received: Jul 7, 2016
Revised: Oct 2, 2017
Accepted: Oct 3, 2017

INTRODUCTION

Direct cell-to-cell communication plays a pivotal role in many aspects of multicellular life, as well as in many disease states. Gap junction (GJ) channels consist of two hemichannels (also termed connexons) that dock head on in the extracellular space, bridging the plasma membranes and thus connecting the cytoplasm of apposed cells. These channels are assembled from four-pass trans-membrane

This article was published online ahead of print in MBoC in Press (http://www.molbiolcell.org/cgi/doi/10.1091/mbc.E16-07-0496) on October 11, 2017.
The authors declare no competing financial interests.
Author contributions: A.F.T. designed experiments, performed experiments, evaluated data, designed figures, wrote the first draft of the manuscript, and edited the manuscript. R.A.M., C.G.F., and R.M.K.-A. performed experiments in response to reviewer critique. M.M.F. designed experiments, evaluated data, edited figures, and revised the manuscript.
†Present address: Department of Biological Sciences, Moravian College, Bethlehem, PA 18018.
*Address correspondence to: Matthias M. Falk (MFalk@lehigh.edu).

Abbreviations used: CHC, clathrin heavy chain; Cx, connexin; GJ, gap junction; GJIC, gap junction intercellular communication; LY, Lucifer yellow; MAGUK, membrane-associated guanylate kinase; MAPK, mitogen-activated protein kinase; PAECs, pulmonary artery endothelial cells; MDCKs, Madin–Darby canine kidney; PBS, phosphate-buffered saline; PKA, protein kinase A; PKC, protein kinase C; PM, plasma membrane; RT, room temperature; ZO-1, zonula occludens-1 protein.

Supplemental Material can be found at:
http://www.molbiolcell.org/content/suppl/2017/10/09/mbc.E16-07-0496v1.DC1

proteins termed connexins (Cxs). Clusters of GJ channels in densely packed arrays, termed GJ plaques, typically consist of hundreds to thousands of individual channels (Bruzzone *et al.*, 1996; Kumar and Gilula, 1996; Falk *et al.*, 2009). Cx43-based GJs are of particular interest because of their ubiquitous expression in most tissues and the central role they play in the heart and vasculature (Lin *et al.*, 2007; Remo *et al.*, 2012; Lambiase and Tinker, 2015; Meens *et al.*, 2015).

A number of independent studies using an array of imaging techniques convincingly demonstrate that newly synthesized GJ channels typically appear to accrue along the outer edge of GJ plaques while older, nonfunctional, and permanently closed GJ channels are removed from plaque centers (Gaietta *et al.*, 2002; Lauf *et al.*, 2002; Falk *et al.*, 2009; Gilleron *et al.*, 2011; Rhett *et al.*, 2011; Nickel *et al.*, 2013). This continuous and dynamic turnover of channels in GJ plaques correlates with the known and unusually short 1–5 h half-life of Cxs and GJs observed in vivo and in situ (with the notable exception of lens fiber cells, which do not maintain functional protein-degradation machinery in order to retain eye lens transparency; Fallon and Goodenough, 1981; Beardslee *et al.*, 1998; Gaietta *et al.*, 2002; Falk *et al.*, 2009, 2014). Dynamic GJ channel renewal also correlates with more recent studies suggesting that only a small portion of channels in a GJ plaque appear to be functional at any given time (Bukauskas *et al.*, 2000; Curti *et al.*, 2012; Flores *et al.*, 2012). Interestingly, continuous GJ channel endocytosis and renewal is important not only for regulating natural levels of GJIC (Kretz *et al.*, 2003; Qiu *et al.*, 2003; Nlend *et al.*, 2006; Wang *et al.*, 2007; Nakano *et al.*, 2008; Remo *et al.*, 2011; Johnstone *et al.*, 2012; reviewed in Laird, 2014; Kelly *et al.*, 2015; Solan and Lampe, 2015; Falk *et al.*, 2016), but also in circumstances where cells physiologically or pathologically separate from each other, such as development, wound healing, mitosis, apoptosis, leukocyte extravasation, ischemia, hemorrhage, edema, and cancer metastasis (Ginzberg and Gilula, 1979; Lo and Gilula, 1979; Leach and Oliphant, 1984; Baker *et al.*, 2008; Gilleron *et al.*, 2008; Boassa *et al.*, 2010; Hesketh *et al.*, 2010; Fong *et al.*, 2014; Nimlamool *et al.*, 2015). However, how GJ biosynthesis, maintenance, and specifically aging and turnover are regulated on a molecular level is not well understood and has been the focus of this investigation.

Cx43 is a well studied phosphoprotein whose function is regulated by a large number of serine (S) and tyrosine kinases and phosphatases that act on Cx43 at multiple sites during all stages of its life cycle. These stages include trafficking from the ER to the Golgi and plasma membrane and altering Cx oligomerization behavior, as well as GJ assembly, gating, internalization, degradation, and regulation of the cell cycle (Thevenin *et al.*, 2013; Solan and Lampe, 2015; Falk *et al.*, 2016). Several of these phosphorylation events have been linked to GJ internalization and turnover (Thevenin *et al.*, 2013; Solan and Lampe, 2014, 2015; Falk *et al.*, 2016). However, a comprehensive understanding of molecular events that regulate channel accrual, GJ plaque assembly, and turnover, or of events that transition functional/open channels into nonfunctional/closed channels that then may become endocytosed, has not been established.

Phosphorylation/dephosphorylation events on specific Cx43 C-terminal residues are also likely to control Cx43's many known interactions with various binding partners, such as chaperones, scaffolding proteins, kinases, phosphatases, ubiquitin ligases, deubiquitinases, and endocytic and other regulatory proteins (Giepmans, 2006; Herve *et al.*, 2012). Precise spatiotemporal control of their binding is crucial, as many of the binding proteins that regulate GJ function likely are not all bound at one time, but are recruited and interact with Cxs only at certain stages of their life cycles (Solan and Lampe, 2007; Thevenin *et al.*, 2013).

One important binding partner of Cx43 in particular, the scaffolding protein zonula occludens-1 (ZO-1), has been characterized in greater detail. ZO-1 is known to interact with GJs (Giepmans and Moolenaar, 1998; Toyofuku *et al.*, 1998) and to bind to the periphery of GJ plaques, where newly synthesized channels accrue (Hunter *et al.*, 2005; Baker *et al.*, 2008). ZO-1 is a member of the membrane-associated guanylate kinase family (MAGUK) of proteins. Cx43 has been shown to interact with the PDZ-2 domain of ZO-1 through its extreme C-terminus, with the last four residues of Cx43 inserting into a binding pocket (Chen *et al.*, 2008; Thevenin *et al.*, 2013). Multiple independent investigations indicate that newly synthesized Cxs traffic to the plasma membrane, dock in the periphery of GJ plaques (the peri-nexus), and accrue to the outer edge of GJ plaques, while simultaneously older channels are internalized from plaque centers (Gaietta *et al.*, 2002; Lauf *et al.*, 2002; Falk *et al.*, 2009; Cone *et al.*, 2014). Rhett *et al.* showed that ZO-1 regulates the Cx43 Cx-to-GJ transition, suggesting that ZO-1-binding to Cxs slows down their accrual rate, and therefore balances GJ plaque size (Rhett *et al.*, 2011). Studies by Chen and colleagues suggest that S373 phosphorylation on a peptide representing the most C-terminal portion of Cx43 protein decreases affinity for ZO-1 eightfold (Chen *et al.*, 2008). This finding was further corroborated by studies of Dunn and Lampe, who demonstrated that under conditions of induced Akt-activation (wounding, hypoxia), phosphorylation of S373 led to detachment of ZO-1 from Cx43 GJs (Dunn and Lampe, 2014), suggesting a possible role of S373 phosphorylation/dephosphorylation in regulating Cx43/ZO-1 interaction. Additional phosphorylation events located in the vicinity of the ZO-1 binding site (e.g., S365 and S368, known respectively as protein kinase A [PKA] and protein kinase C [PKC] targets; Solan and Lampe, 2007); farther upstream in the Cx43 C-terminal domain (e.g., S255; S262, not conserved in humans; S279/S282, all known MAPK target sites); and located in the vicinity of the Cx43 internalization signals (S2, $Y^{265}AVF^{268}$; S3, $Y^{286}KLV^{289}$) (Thomas *et al.*, 2003; Fong *et al.*, 2013) are also implied to contribute to GJ turnover (Johnson *et al.*, 2013; Fong *et al.*, 2014; Nimlamool *et al.*, 2015; Spagnol *et al.*, 2016). However, a sufficient understanding of how dynamic Cx43/ZO-1 binding and release is regulated on a molecular basis and how ZO-1 binding and disengagement relates to other Cx43 modifications that aid to transition functional/open into nonfunctional/closed GJ channels that lead to endocytosis is currently lacking.

To address this issue, we constructed and analyzed a series of phosphomimetic and phosphorylation-dead mutants in which multiple known S residues of the Cx43 C-terminal domain were mutated into glutamic acid (E) or alanine (A) residues. We expressed the mutants as native proteins (i.e., not fused to green fluorescent protein [GFP] or any other tag) in Cx-deficient HeLa and Madin–Darby canine kidney (MDCK) epithelial cells, and investigated whether 1) the mutants were translated into stable, full-length Cx43 polypeptides, 2) the mutants were able to form GJ plaques, 3) plaques still interacted with ZO-1, 4) Cx43/ZO-1 interaction was altered, 5) amounts of ZO-1 bound to the Cx43 mutants were modified, 6) GJ plaque size and number was different, 7) Cx43 mutant protein half-life was affected, 8) the endocytic rate of the mutated Cxs was altered, and 9) channel function (Lucifer yellow [LY] dye-transfer ability) was increased or decreased. Together with previous reports, our results presented here indicate that a series of hierarchical phosphorylation/dephosphorylation events at S373, S365, and S368 (known Akt, PKA, and PKC sites, respectively) regulate—through ZO-1 binding and its release—Cx docking, channel accrual, and transitioning of peripherally located functional (open) into centrally located nonfunctional (closed) GJ channels that can then be endocytosed.

RESULTS

Generation and expression of Cx43 constructs mutated at specific C-terminal serine residues

To determine whether attachment or detachment of ZO-1 to/from the Cx43 C-terminus may be regulated by phosphorylation of the Cx43 C-terminal domain, we generated a series of mutants in which several known regulatory S residues in the Cx43 C-terminus were exchanged (Figure 1A). Both phosphorylation-mimetic (serines, S, replaced with glutamic acid, E) and phosphorylation-dead (S replaced with alanine, A) mutants were generated. Sites known to be phosphorylated by Akt (S373), PKC (S368), PKA (S365), and MAPKs (S255, S279/S282) were targeted in this study (Figure 1B) (Solan and Lampe, 2007, 2014; Thevenin *et al.*, 2013). All mutants were constructed untagged, as tagging Cx43 with a fluorescent probe, such as GFP on its C-terminus, is known to prevent Cx43 from interacting with ZO-1 (Hunter *et al.*, 2005; Thevenin *et al.*, 2013). All Cx43 constructs produced stable, correct–molecular mass protein products in addition to known Cx43-phosphorylation forms (P0, P1, P2) in Cx-deficient HeLa and MDCK cells (shown for MDCK cells and compared with endogenously Cx43-expressing pulmonary artery endothelial cell (PAEC) controls, Figure 1C) (Solan and Lampe, 2007, 2009; Thevenin *et al.*, 2013). Under conditions applied, transfection efficiencies and resulting Cx43 protein levels were much higher in MDCK compared with HeLa cells (~90% and 25% transfection efficiencies, respectively) (compare Figure 2 and Supplemental Figure S1, as well as Figure 3, A and B, with Figure 3C). In addition, all mutants assembled efficiently into GJ plaques when expressed in HeLa or MDCK cells (Figure 3 and Supplemental Figure S1). In general, GJ plaques formed in HeLa cells were larger than plaques assembled in MDCK cells, consistent with a generally higher metabolic activity of these cancer cells. However, GJ plaque number per cell was increased in MDCK cells in a zipperlike morphology more similar to the morphology of GJs formed by endogenously expressed Cx43 in situ, or in primary cells (compare Figure 2 and Supplemental Figure S1). We therefore performed morphological plaque analyses (size measurements and interaction with ZO-1, shown in Figure 2) primarily in HeLa cells, as larger plaques are more accessible to light microscopic analyses, while biochemical and functional analyses (shown in Figures 3–7) were performed primarily in MDCK cells. However, comparable results for all experiments were obtained in both cell lines.

Mutating Cx43 serines 365, 368, and 373 totally alters the distribution of ZO-1 on GJ plaques

To investigate Cx43/ZO-1 interactions, Cx43 S mutants were expressed in HeLa cells, Cx43 and ZO-1 proteins were coimmunostained, and GJ plaques were analyzed by high-resolution confocal fluorescence analyses (Figure 2). Cells expressing wild-type (WT) Cx43 exhibited the typical staining of ZO-1 along the outer periphery of GJ plaques, as reported previously by others and our own laboratory (Figure 2A, panels in row 1; Hunter *et al.*, 2005; Baker *et al.*, 2008). In contrast, both the A and E mutants of S365, S368, and S373 displayed a completely different distribution pattern of ZO-1 on Cx43 GJ plaques: In S365A/E, S368A/E and S373A mutants, ZO-1 was no longer restricted to the periphery, but was distributed over the entire plaque surface (Figure 2A, rows 2–6), while the S373E mutant no longer exhibited any detectable interaction with ZO-1 (Figure 2A, row 7). All described results were supported by linescan analyses (performed along the dotted white lines shown) for both green (Cx43), and red (ZO-1) fluorescence channels (Figure 2A, right panels). This result is in agreement with in vitro Cx43/ZO-1-PDZ2 peptide binding studies performed by Chen *et al.* (2008), as well as more recent work by Dunn and Lampe (2014). To clearly distinguish plaque peripheries from plaque centers and avoid potential image processing artifacts, only plaques viewed on their plane surfaces, were analyzed; plaques oriented edge-on were not considered. In addition, quantifying remaining levels of ZO-1 in the cytoplasm correlated well with amounts of ZO-1 bound to GJ plaques in each mutant. Mutants that showed ZO-1 binding throughout plaques (S365A/E; S368A/E; S373A) exhibited correspondingly lower cytoplasmic ZO-1 levels compared with WT and the S373E mutant (Figure 2B).

To test whether mutating other S residues elsewhere in the Cx43 C-terminal domain would have a similar effect on Cx43/ZO-1 interactions, we mutated three additional known regulatory S residues: S255, S279, and S282 (279/282 together). Both A and E mutants at these sites displayed normal distributions of ZO-1 along the rim of GJ plaques that were similar to WT (Figure 2C). This result suggests

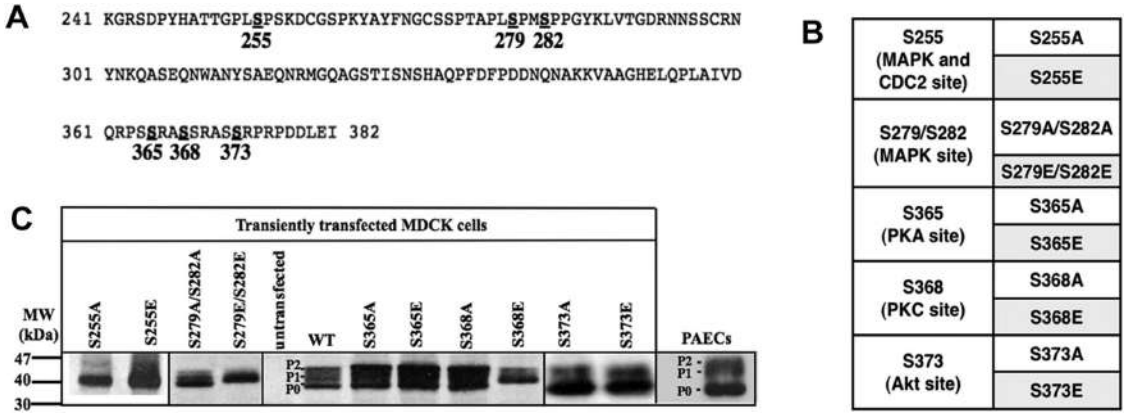

FIGURE 1: Cx43 serine (S) mutants are translated into stable, full-length proteins. (A) Amino acid sequence of the rat Cx43 C-terminal domain (residues 241–382) with S residues mutated into A and E in this study, in bold. (B) Summary of the generated S to alanine (A) and aspartic acid (E) mutants, including the kinases known to phosphorylate these sites. CDC2 (cell-dependent control 2; also known as cyclin-dependent kinase 1). (C) Cx43 Western blot analysis of lysates of MDCK cells transiently expressing the Cx43 S constructs. All mutants translated into full-length proteins. Note that all mutants were expressed as native proteins, not fused to GFP or any other tag. PAECs expressing endogenous Cx43 were analyzed in parallel as positive control. Positions of known Cx43 phosphorylation forms (P0, P1, P2) are indicated.

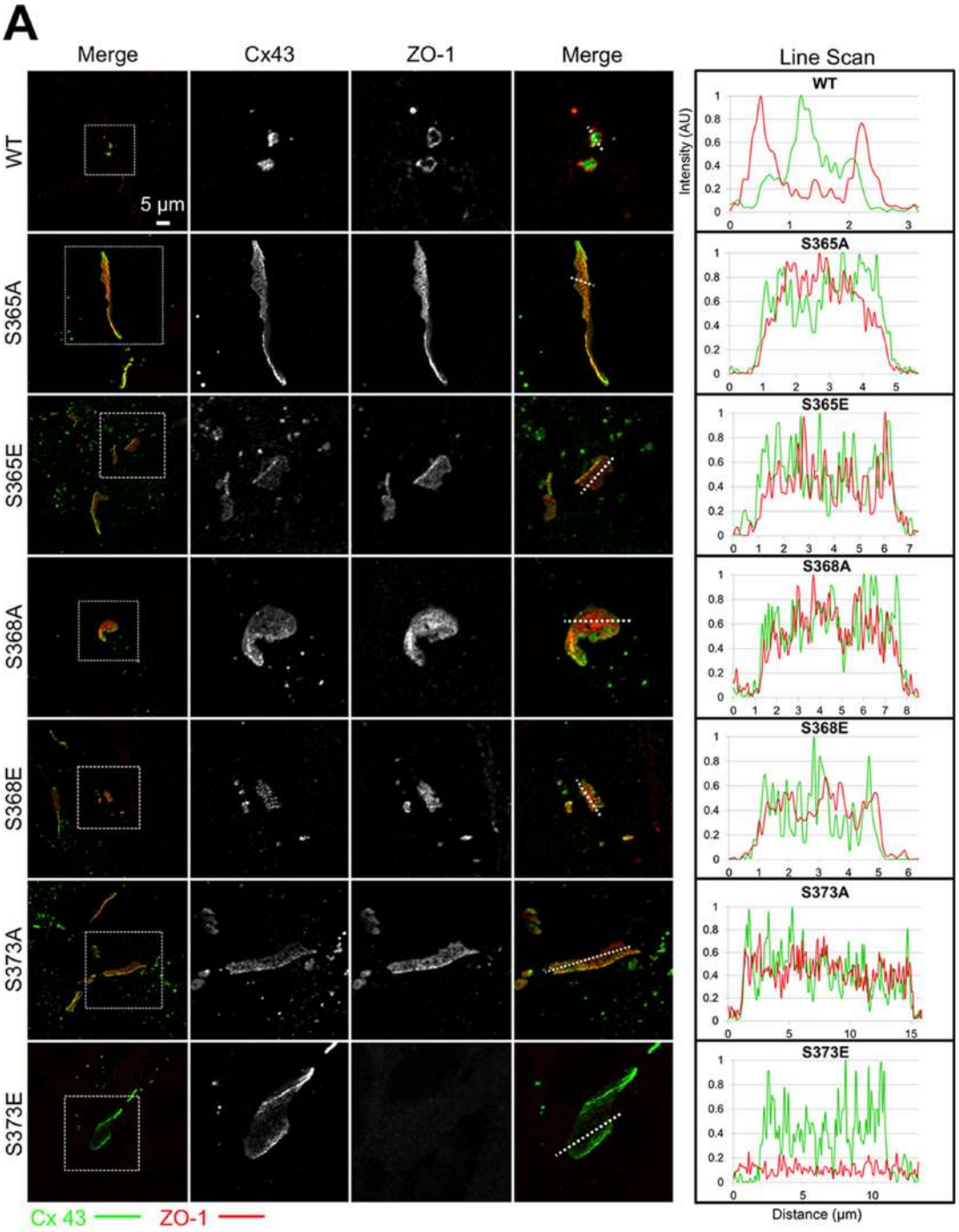
A
Merge
Cx43
ZO-1
Merge
Line Scan
WT
S365A
S365E
S368A
S368E
S373A
S373E
5 µm
Intensity (AU)
Distance (µm)
Cx 43
ZO-1
B
GJ-bound ZO-1
Cytosolic ZO-1
Total ZO-1 Protein Levels
100%
80%
60%
40%
20%
0%
***
***
**
ns
**
ns
WT
S365A
S365E
S368A
S368E
S373A
S373E

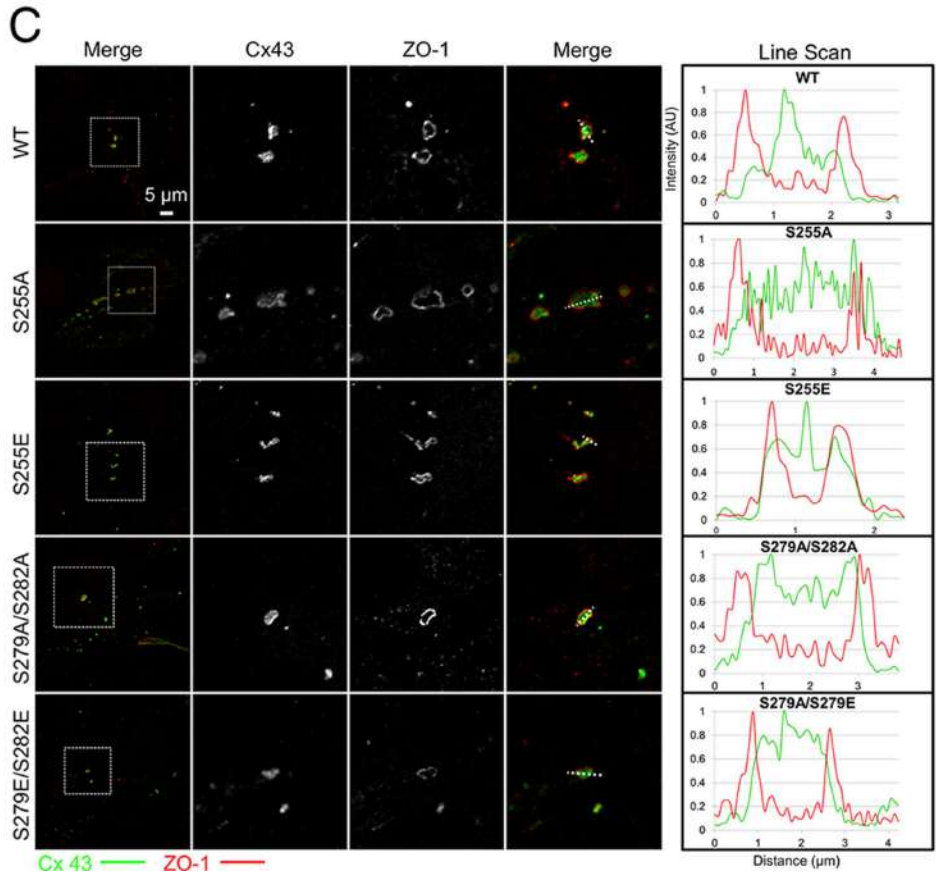

FIGURE 2: Mutating S365, S368, and S373, but not S255 and S279/S282, in Cx43 causes a dramatically altered ZO-1 distribution on GJs. HeLa cells expressing WT and respective Cx43 S mutants were processed for immunofluorescence analyses 24 h posttransfection and high-resolution confocal analyses. In the merged images, labeled Cx43 is shown in red and ZO-1 in green. Representative images of *en face* GJ plaques are shown in A and C. Boxed regions selected in the left panel are shown magnified in the panels to the right. Cx43 and ZO-1 fluorescence signals recorded along the dotted lines traversing GJ plaques are shown in the line scan graphs on the right. (A) In WT Cx43, ZO-1 is distributed only along the periphery of GJ plaques, in accordance with previous observations (Baker *et al.*, 2008; Hunter *et al.*, 2005). In contrast, in S365A and E, S368A and E, and S373A mutants, ZO-1 is distributed throughout plaques, while the S373E mutant does not bind ZO-1 at all. (B) Quantitative analyses of ZO-1 bound to GJ plaques and distributed in the cytoplasm (as a percentage) averaged from at least three independent experiments. Average percentages of ZO-1 levels were calculated from at least 20 images. Error bars are SEM. One-way ANOVA, followed by Dunnett multiple comparison analyses (compared with the WT), is shown. (C) Mutating S255, S279, and S282 in Cx43 into A or E did not alter ZO-1 distribution, resulting in the rim staining typical for WT Cx43.

that only S residues in the vicinity of the ZO-1 binding site regulate ZO-1 binding and release, while S residues located farther upstream (known MAPK sites located juxtaposed to the endocytic motifs S2 and S3; Fong *et al.*, 2013) have no effect. Similar analyses performed with high-resolution wide-field fluorescence microscopy (150× primary magnification, Supplemental Figure S2), or AiryScan confocal superresolution microscopy (up to 140 nm resolution in *X*–*Y*, shown for representative mutants S255A and S365A, Supplemental Figure S3) showed comparable ZO-1/GJ plaque distribution patterns consistent with our high-resolution confocal analyses.

Cx43/ZO-1 coimmunoprecipitation correlates with altered ZO-1/GJ plaque distribution

To further investigate altered mutant Cx43/ZO-1 colocalization, we first performed coimmunoprecipitation analyses of Cx43 and ZO-1 from whole-cell lysates. Coimmunoprecipitation of ZO-1 from HeLa cells expressing WT or Cx43 mutants showed that indeed, significantly more ZO-1 interacted and coprecipitated with S365A and E, S368A and E, and S373A mutants, while significantly less ZO-1 coprecipitated with the S373E mutant when analyzed by one-way analysis of variance (ANOVA) with Dunnett comparison test) (Figure 3, A and B).

To further refine our analyses and investigate whether increased/decreased ZO-1 coprecipitation indeed was specific for Cx43 localized in GJ plaques, we performed Triton X-100 solubility assays in Cx43 WT and mutant transfected MDCK cells. Based on the known resistance of GJs to dissolving in 1% Triton X-100 (Musil and Goodenough, 1991), plasma membrane GJs can be separated from the intracellular Cx43 pool (cCxs, Cx43 polypeptides). First, we found that much more ZO-1 was present in the insoluble than in the soluble fractions (Figure 3C). In addition, the level of ZO-1 that coprecipitated with S365A and E, S368A and E, and S373A mutants was increased, while the S373E mutant bound less ZO-1 than WT Cx43 GJs, consistent with our previously described fluorescence colocalization analyses (Figure 3C, top panel). Also note that Cx protein levels of mutant Cxs were increased (Figure 3C, bottom panel),

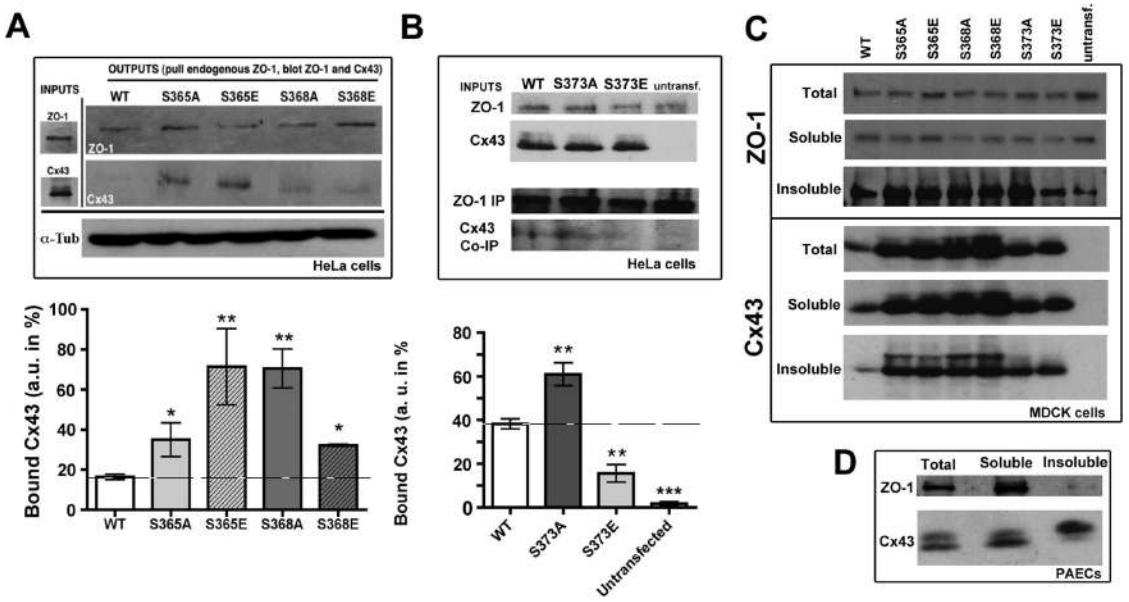

FIGURE 3: In S mutants that bind ZO-1 throughout GJ plaques, many more Cx43 polypeptides are bound to and coprecipitate with ZO-1 than for WT Cx43. (A, B) HeLa cells were transfected with Cx43 WT and S mutants and processed 24 h later for coimmunoprecipitation analyses. Whole-cell lysates were incubated with anti-ZO-1 antibodies and samples were tested for both ZO-1 and Cx43 after SDS–PAGE and Western blot analyses. Representative gels are shown in A and B, and quantitative analyses (as percentages) of at least three independent analyses, followed by one-way ANOVA with a Dunnett multiple comparison test (compared with the WT), are shown below. Note that S mutants S365A and E, S368A and E, and S373A all coprecipitated significantly more Cx43 than did WT, while the S373E mutant coprecipitated significantly less. Untransfected HeLa cells not endogenously expressing Cx43 were analyzed in parallel. (C) In parallel, Triton X-100 solubility assays according to Musil and Goodenough (1991) were performed in Cx43 WT and mutant expressing MDCK cells 24 h posttransfection. Cells were lysed in buffer containing 1% Triton X-100 and centrifuged at 10,000 × *g* to separate cell nuclei and mitochondria. Supernatants were then centrifuged at 100,000 × *g* to separate plasma membrane GJs (insoluble) from cytoplasmic Cx43 (soluble). After SDS–PAGE and Western blot, samples were analyzed for both Cx43 and ZO-1. Comparable results were obtained. (D) Triton X-100 solubility assays were carried out in parallel as a positive control in endogenously Cx43-expressing primary PAE cells.

consistent with increased protein half-life and impaired mutant protein turnover rates (see below). Similar results were also obtained when fractionation assays were performed in HeLa cells, albeit with a somewhat higher level of background due to the significantly lower transfection efficiency and thus overall lower Cx43 protein expression level in these cells (Supplemental Figure S4).

In addition, as a control, we separated whole cell lysates derived from primary PAECs that express Cx43 endogenously at high levels into soluble and insoluble fractions (Figure 3D). Also, in these cells, much more ZO-1 was present in insoluble than in soluble fractions. In addition, in agreement with the concept that Cx43 in GJs is highly phosphorylated compared with soluble (intracellular, secretory) Cx43 (Solan and Lampe, 2009), insoluble GJ Cx43 polypeptides migrated more slowly, compared with the soluble Cx43 protein pool. Taken together, these biochemical data fortify our coimmunofluorescence data, further supporting our conclusion that ZO-1 remains bound to Cx43 when critical Cx43 S residues are mutated.

Cx43 mutants that cannot disengage from ZO-1 form significantly larger GJ plaques

Because ZO-1 has been found to be involved in regulating GJ plaque size (Hunter *et al.*, 2005; Rhett *et al.*, 2011), we next assessed the effect of our S mutagenesis on mutant Cxs to form GJ plaques (total GJ plaque area/cell pair) and on Cx protein half-life. HeLa cells expressing WT or mutant Cx43 and immunostained with Cx43 antibodies were imaged and the Cx43 fluorescence signal at cell–cell contacts was quantified using ImageJ software (Figure 4, A and B; see Supplemental Figure S6 for details). Levels of GJ Cx43 at cell–cell contacts in S368E and S373E mutants were comparable to that in WT Cx43, while all other mutants (S365A and E, S368A, S373A) displayed significantly more GJ plaque area (indicated by significantly increased fluorescence levels) than WT Cx43 (Figure 4, A and B). These results concur with the observed ZO-1 distribution differences presented in Figure 2, A and B, signifying that the S368E and S373E mutants accurately replicate steps that occur in aging GJ plaque channels—namely, that Cx43/ZO-1 interaction is naturally abolished, leading to reduced plaque size in these mutants. This is in contrast to the Cx43 mutants that prevent normal ZO-1 detachment, leading to increased overall GJ plaque area in these mutants. When any of our mutants were expressed with a C-terminal GFP tag, observed plaque size-differences were no longer detectable (unpublished data), further supporting the findings of Hunter *et al.* (2003, 2005) and Rhett *et al.* (2011) that Cx43/ZO-1 interaction regulates channel accrual/GJ plaque size.

Cx43 mutants with altered ZO-1 interaction profiles have drastically increased protein half-lives

To ascertain whether Cx43 protein half-life was affected in our mutants, MDCK cells expressing WT or mutant Cx43 were treated with cycloheximide to inhibit protein biosynthesis and remaining levels of Cx43 polypeptides were analyzed by Western blot analyses using Cx43-specific antibodies (Figure 5). All mutants, except S373E (5.3 h), were found to have significantly longer protein half-lives (~12–21 h)

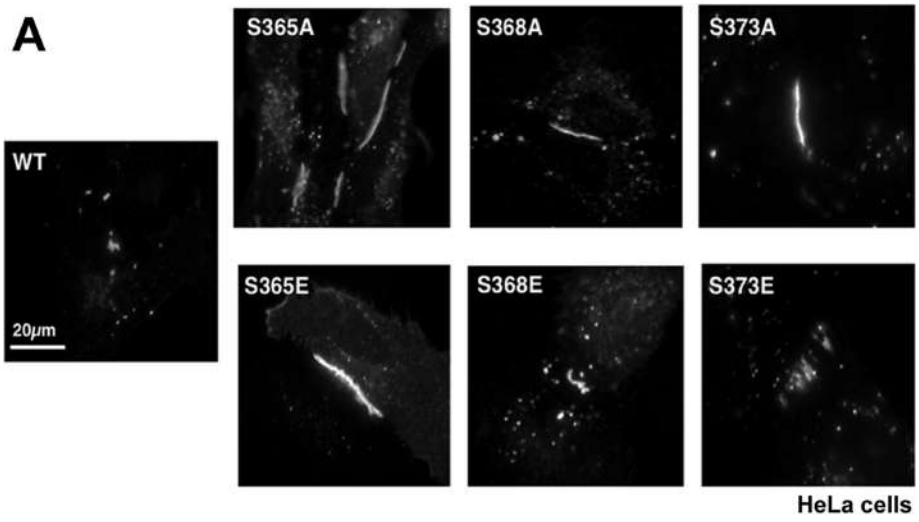

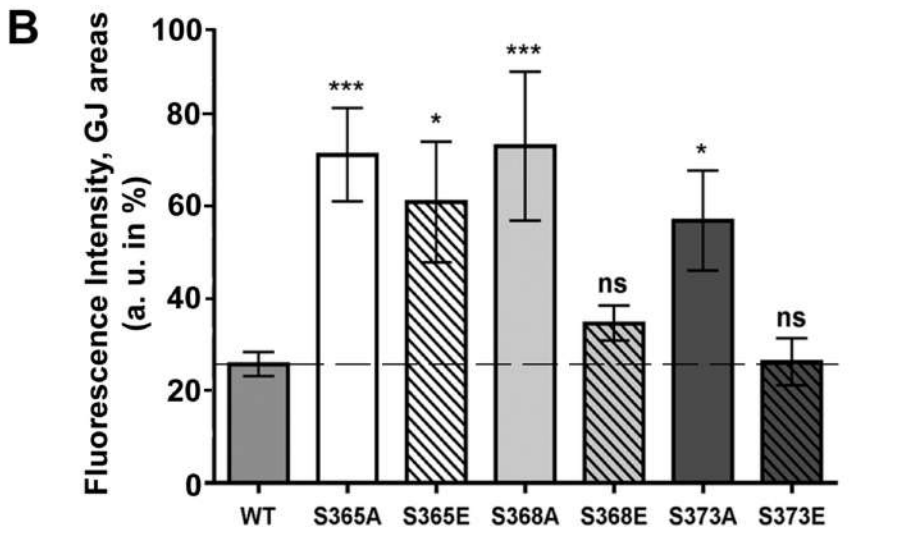

FIGURE 4: S mutants that bind ZO-1 throughout GJ plaques in general form more and larger GJ plaques. HeLa cells were transfected with Cx43 WT and mutant constructs and processed 24 h posttransfection for Cx43-immunofluorescence analysis. Representative images are shown in A. Quantitative analyses (as percentages) of GJ plaque area fluorescence of three independent experiments with a total of 70-80–measurements are shown in B. Error bars represent the SEM. One-way ANOVA followed by Dunnett multiple comparison test results is shown for all mutants, as compared with WT Cx43. Note that Cx43 GJ fluorescence is significantly increased in S365A and E, S368A, and S373A mutants.

compared with WT Cx43 (4.3 h). Taken together, increased Cx43 protein half-lives and increased GJ levels at plasma membrane cell–cell contacts suggests either 1) that the ability of the S365A and E, S368A and E, and S373A mutants to engage/disengage from ZO-1 is perturbed, resulting in an inappropriate regulation of GJ channel accrual; or 2) that these S mutants are endocytosed more slowly.

Increased mutant GJ plaque size results from increased channel accrual, rather than decreased endocytosis rates

To determine whether mutants exhibiting longer protein half-lives and/or increased GJ plaque size/numbers have decreased endocytosis rates, we conducted coimmunoprecipitation analyses of clathrin heavy chain (CHC) and Cx43 in MDCK cells (Figure 6). Previously, Cx43-based GJs have been shown to internalize using the clathrin endocytic machinery (Piehl *et al.*, 2007; Gumpert *et al.*, 2008; Fong *et al.*, 2013); hence levels of clathrin bound to Cx43 can be used as a reliable measure to gauge the rate of GJ internalization (Gumpert *et al.*, 2008; Fong *et al.*, 2014). None of the mutants revealed significantly altered clathrin-binding levels from those in WT (Figure 6, A and B). These results argue against a reduced endocytosis rate, and instead argue for an increased channel accrual rate caused by a disregulation in Cx43/ZO-1 binding and release characteristics in these S mutants.

GJ channels assembled from Cx43 mutants that cannot disengage from ZO-1 stay functional (open)

To test whether our Cx43 S mutants also exhibit altered channel activities, we performed scrape-loading Lucifer yellow (LY) dye-transfer assays in Cx43 WT or mutant-expressing MDCK cells (Figure 7). The extremely high transfection rate of MDCK cells (app. 90%; see *Material and Methods*) allowed us to perform these assays in transiently transfected cells. Distance of LY spreading away from the scrape 10 min past injury and fixation was determined by quantitatively measuring LY-fluorescence signals. LY in Cx43 WT-expressing MDCK cells exhibited robust dye transfer rates (~100 μm/10 min; ~4 cell width) compared with those in untransfected MDCK cells that were tested in parallel as negative controls. These cells took up the dye but were not able to spread it to neighboring cells (~25 μm/10 min; ~1 cell width) (Figure 7, A and B, panels 1 and 2).

The S365A mutant showed no difference in dye transfer from WT Cx43 (~100 μm/10 min; ~4 cell width), while in contrast, the S365E mutant (simulating permanent S365 phosphorylation) exhibited a significantly increased level of dye transfer and the highest of all mutants tested (~135 μm/10 min; ~$5^1/_2$ cell width) (Figure 7, A and B, panels 3 and 4). This result conforms to the proposed role of S365 and S368 in regulating transition from functional (open) into nonfunctional (permanently closed) channels that is controlled by S365 dephosphorylation/S368 phosphorylation ("gatekeeper event"; Solan and Lampe, 2007). In a Cx43 mutant in which S365 cannot be phosphorylated (as in the S365A mutant), phosphorylation of S368 likely can occur unperturbed and channels mature into nonfunctional (closed) channels normally, as in the WT. However, when permanent phosphorylation of S365 is simulated (as in the S365E mutant), concomitant phosphorylation of S368 cannot occur, resulting in channels staying functional (open). A similar result was also obtained with the S368A mutant, where LY transfer levels were almost as high as in the S365E mutant (~120 μm/10 min; ~5 cell width) (Figure 7, A and B, panel 5), again indicating that preventing S368 phosphorylation prevents channels from permanently closing. Accordingly, the S368E mutant exhibited the lowest dye transfer capability of all mutants (~50 μm/10 min; ~2 cell widths) (Figure 7, A and B, panel 6).

The S373E mutant also transferred LY at a significantly lower rate than for WT Cx43 (~75 μm/10 min; ~3 cell widths) (Figure 7, A and B, panel 8). This result is in agreement with our plaque size analyses

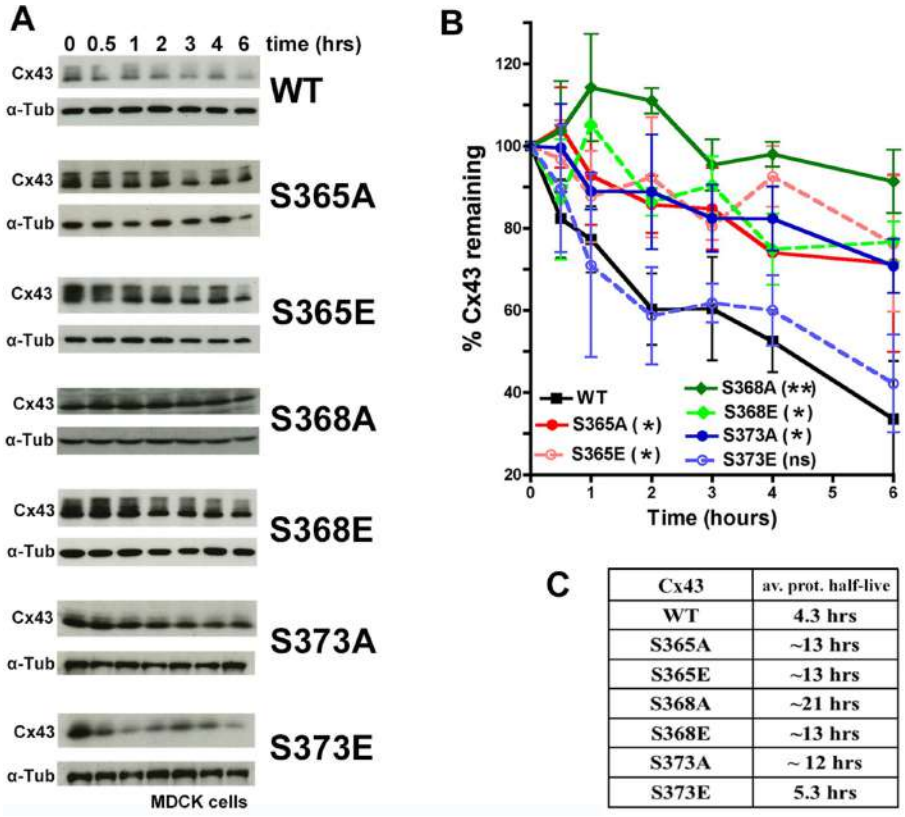

Cx43	av. prot. half-live
WT	4.3 hrs
S365A	~13 hrs
S365E	~13 hrs
S368A	~21 hrs
S368E	~13 hrs
S373A	~ 12 hrs
S373E	5.3 hrs

FIGURE 5: Cx43 S mutants that cannot disengage from ZO-1 have significantly longer protein half-lives. MDCK cells were transfected with WT or mutant Cx43 constructs and treated 20 h posttransfection with cycloheximide to inhibit protein biosynthesis. (A) Levels of Cx43 protein remaining at indicated time points were analyzed after cell lyses by Western blot using anti-Cx43 antibodies. Equal loading was controlled by stripping membranes and reprobing with anti α-tubulin (α-Tub) antibodies. Representative gels are shown. (B) Quantitative blot analyses of at least three independent experiments. Error bars represent the SEM. One-way ANOVA followed by Dunnett multiple comparison test results is shown for all mutants, as compared with WT Cx43. (C) Summarized average protein half-lives for all mutants. Owing to extremely prolonged half-lives of S365A and E, S368A and E, and S373A mutants, values were extrapolated and therefore are approximate.

(with this mutant not forming a larger GJ plaque area than for WT; Figure 4) and ZO-1 redistribution results (with this mutant being unable to interact with ZO-1; Figure 2, A and B), supporting the concept that S373 is phosphorylated early after biosynthesis in Cx43 Cxs concomitant with transport to the plasma membrane. Owing to its inability to interact with ZO-1, in this mutant the ability to assemble GJ plaques appears to be perturbed. Indeed, in MDCK cells expressing the S373E mutant, many cell–cell borders did not exhibit detectable GJs (Supplemental Figure S1). Taken together, our results indicate that GJ assembly, channel function, and maturation into nonfunctional channels correlate with ZO-1 binding and release, and that these critical regulatory steps are controlled by a series of phosphorylation/dephosphorylation events that occur in a sequential order on S373, S365, and S368 in the Cx43C-terminal domain.

DISCUSSION

We found that mutating single amino acid residues in the Cx43 C-terminal domain can dramatically alter the distribution of a well-known Cx43 binding partner, ZO-1, from its distinct localization restricted to the peripheral rim of WT GJ plaques (Hunter *et al.*, 2003, 2005; Baker *et al.*, 2008; Rhett *et al.*, 2011) into a pattern that suggests binding of ZO-1 throughout the entirety of GJ plaques, or into a complete loss of binding. These critical amino acid residues represent prominent S residues (S373, S368, S365) that are well known to regulate GJ function via their phosphorylation states. Mimicking phosphorylation/dephosphorylation of these residues by mutating them into phosphomimetic and phospho-dead residues (glutamic acid [E] or alanine [A], respectively) lead to these dramatic changes in ZO-1 binding, suggesting that specific phosphorylation/dephosphorylation events occurring on critical Cx43 S residues located in the vicinity of the C-terminal Cx43 ZO-1 binding site regulate Cx43/ZO-1interaction, and if phosphorylation on these residues is permanently prevented (as in the S to A mutants) or simulated (as in the S to E mutants), ZO-1 no longer can bind, or can no longer disengage from Cx43 and remains bound throughout the mutant GJ plaques. Notably, similarly mutating regulatory S residues located farther upstream in the Cx43 C-terminal domain (S279, S282, S255 phosphorylated by MAPK) did not at all affect ZO-1 localization, and the pronounced rim association typical for WT Cx43 remained. Inability of mutant Cx43 to disengage from ZO-1 correlated with increased Cx43 mutant protein half-life, increased GJ plaque size and number, and reduced LY dye transfer ability, suggesting that disengagement of Cx43 from ZO-1 is necessary for normal GJ function, including transitioning GJ plaque channels from functional (open) into nonfunctional (permanently closed), which then may become endocytosed. Interestingly, phosphorylation/dephosphorylation on S373 and S365 appears to activate channel function (opens channels), while phosphorylation on S368 (and subsequent phosphorylations on upstream MAPK sites) appears to inactivate it (closes channels) and to transition channels for endocytosis. Obtained results correlate well with the described short half-lives of Cxs and GJs (Berthoud *et al.*, 2004), and with previous findings that indicate that i) Cx43 phosphorylation on S373 regulates channel accrual (Dunn and Lampe, 2014), ii) dephosphorylation on S365 followed by phosphorylation on S368 regulates cell–cell coupling efficiency (Solan *et al.*, 2007), and iii) GJ channels that are phosphorylated on S368 remain permanently closed and are endocytosed from central plaque areas (Cone *et al.*, 2014). However, a link between down-regulation of GJIC (which also can be achieved via channel closure) and GJ internalization, and the sequence and type of molecular events that regulate these transitional steps have never been established previously.

With at least 15 different known phosphorylation sites being present in the Cx43 C-terminal domain and multiple protein kinases known to phosphorylate these sites (Solan and Lampe, 2005, 2007, 2009; Thevenin *et al.*, 2013), it appears likely that many of the transitional steps that regulate GJ turnover, including Cx docking and channel accrual, opening and permanently closing GJ channels, and transitioning of functional (open) into nonfunctional (permanently closed) GJ channels, which then may be primed for clathrin-binding

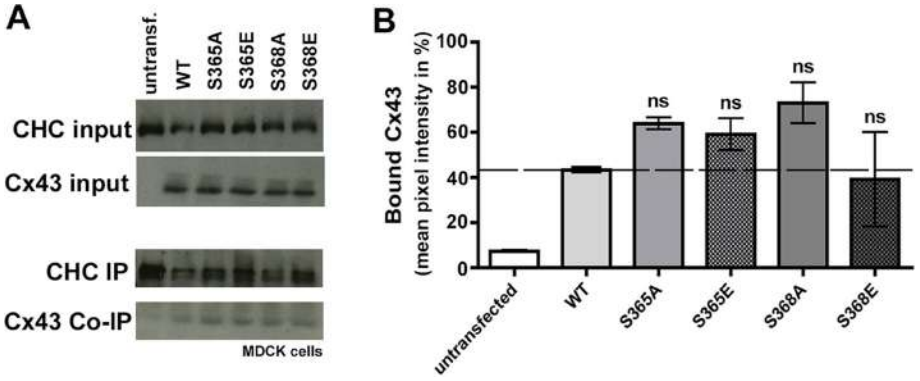

FIGURE 6: Increased Cx43 mutant GJ plaque area likely results from increased channel accrual rather than decreased GJ endocytosis. (A) Cx43 WT and S365 and S368 A and E mutants were expressed in MDCK cells and lysed 24 h later. Cell lysates (including untransfected MDCK cells in controls) were subjected to coimmunoprecipitation analyses using anti-CHC specific antibodies. Amounts of CHC and Cx43 in the lysates (inputs), besides precipitated CHC (IP) and coprecipitated Cx43 (Co-IP), were analyzed. Representative gels are shown. (B) Quantitative Western blot analyses (as percentages) of Cx43 that coprecipitated with CHC are shown. Error bars represent the SEM. One-way ANOVA followed by Dunnett multiple comparison test results are shown for all mutants, as compared with WT Cx43.

and endocytosis, are regulated by distinct Cx phosphorylation events. As phosphomimetic and phospho-dead mutants bear the ability to arrest the Cx43 life-cycle at a relevant critical step, generating and analyzing these mutants allowed us to investigate the role each of these regulatory S residues may have in this process. Instead, activating/inactivating kinases/phosphatases, for example, via wounding or the generation of reactive oxygen species (ROS), may not have allowed us to do these analyses comparably well, as the latter approach is more likely to generate additional, unintentional, and potentially misleading phosphorylation events. In addition, it allowed us to investigate individual phosphorylation events under physiological, non–stress-induced conditions. Further evaluating Cx43S/E mutants together with previously published data finally permitted us to conclude i) that binding of ZO-1 to Cx43 and its subsequent release are regulated by Cx43 phosphorylation; ii) that disengagement from ZO-1 seems necessary for the transition of functional (open) channels into nonfunctional (closed) channels that then may be modified further to permit their endocytosis; and iii) that these transitional GJ channel activation and inactivation steps are regulated by a series of hierarchical phosphorylation/dephosphorylation events that occur on S373, S365, and S368, well-known Cx43 Akt, PKA, and PKC phosphorylation sites (schematically depicted in Figure 8).

Two S residues located in the Cx43 C-terminal domain, in particular, were found previously to play a critical role in regulating GJ channel function. S365 dephosphorylation (phosphorylated by PKA), termed "gatekeeper event" by the Lampe and Sorgen labs, was determined to be critical for successive phosphorylation of S368 (phosphorylated by PKC), an event that was linked to inhibition of GJIC, GJ channel closure, movement of channels to plaque centers, and the loss of GJ plaques from plasma membranes (Cone *et al.*, 2014). S365 phosphorylation is constitutive in the heart, but is absent during hypoxia (Solan and Lampe, 2007). In addition, phosphorylation of S368 is increased in the heart undergoing hypoxia and Cx43 is lost from intercalated discs, suggesting that S368 phosphorylation might trigger GJ channel closure and potentially Cx43 internalization (Solan and Lampe, 2007; Cone *et al.*, 2014), a hypothesis that concurs with our data.

Moreover, several labs previously gained evidence suggesting that phosphorylation/dephosphorylation of S373 in Cx43 (phosphorylated by Akt) may play an important role in regulating Cx43/ZO-1 interaction (Chen and Sudol, 1995; Park *et al.*, 2006, 2007; Rhett *et al.*, 2011; Dunn and Lampe, 2014). Our analyses indeed indicate that phosphorylation at S373 (mimicked in the S373E mutant) averted Cx43/ZO-1 interaction, while preventing S373 phosphorylation (mimicked in the S373A mutant) significantly increased Cx43/ZO-1 interaction (Figures 2 and 3). Some discrepancy, however, seems to remain as to whether S373 phosphorylation actually increases or decreases GJIC (Dunn and Lampe, 2014, and our study). Dunn and Lampe previously gained evidence that suggests that phosphorylation of S373 increases GJ size and cell–cell communication (Dunn and Lampe, 2014), while in our study S373 phosphorylation decreased communication (GJ plaque area remained unchanged in our study, Figures 4 and 7). These contradictory results may be explained by differing experimental conditions, as Dunn and Lampe's experiments were performed under stress conditions (heart injury, hypoxia), which likely lead to strong activation of Akt, while our experiments were performed under normal, unstressed conditions where Akt kinase activity is expected to remain much lower. Importantly and independent of this difference, with respect to the S residue that regulates Cx43/ZO-1 interaction (S373), both our and the Dunn and Lampe studies concur.

Our comprehensive S mutagenesis further indicated that additional S residues are involved in the regulation of Cx43/ZO-1 interaction and GJ channel function. Indeed, dephosphorylation of S373 (which is thought to occur after Cxs have arrived at the plasma membrane and docked to form GJ channels) may not be sufficient to render the newly accrued channels fully functional. Our LY dye transfer experiments indicate that the S373A mutant transfers dye comparably efficiently to WT and S365A mutant (Figure 7), while phosphorylation of S365 (mimicked in the S365E mutant, and reiterated in the S368A mutant, in which phosphorylation of S368 is prevented) resulted in significantly increased dye transfer abilities. Together with our evidence that the S368E mutant is unable to significantly transfer dye, and thus channels in this mutant apparently largely stay closed, our results are in good agreement with those of Solan and colleagues, who also found that phosphorylation of S365 keeps channels open, while phosphorylation of S368 closes channels (Solan *et al.*, 2007).

So why after all may ZO-1's release from GJ channels be required for their endocytosis? The work of Chen *et al.* (2008) indicates that the Cx43/ZO-1 interaction requires that two ZO-1 proteins undergo a structural dimerization known as "domain swap" as they bind two separate Cx43 polypeptides, a structural modification believed to make the PDZ-2 domain interaction of ZO-1 Cx43 specific. Thus, at least two ZO-1 proteins appear to bind to a Cx43 channel in a GJ plaque. As ZO-1 is a very large 220-kDa protein (almost the size of an entire Cx43-based Cx), its dimerization will generate a 440-kDa protein complex that in comparison dwarfs the size of the underlying bound connexon. Likely these huge ZO-1 protein complexes will efficiently shield the cytoplasmic surface of GJ plaques and will need to be removed before subsequent Cx43 modifiers (MAPKs, E3-Ub ligases,

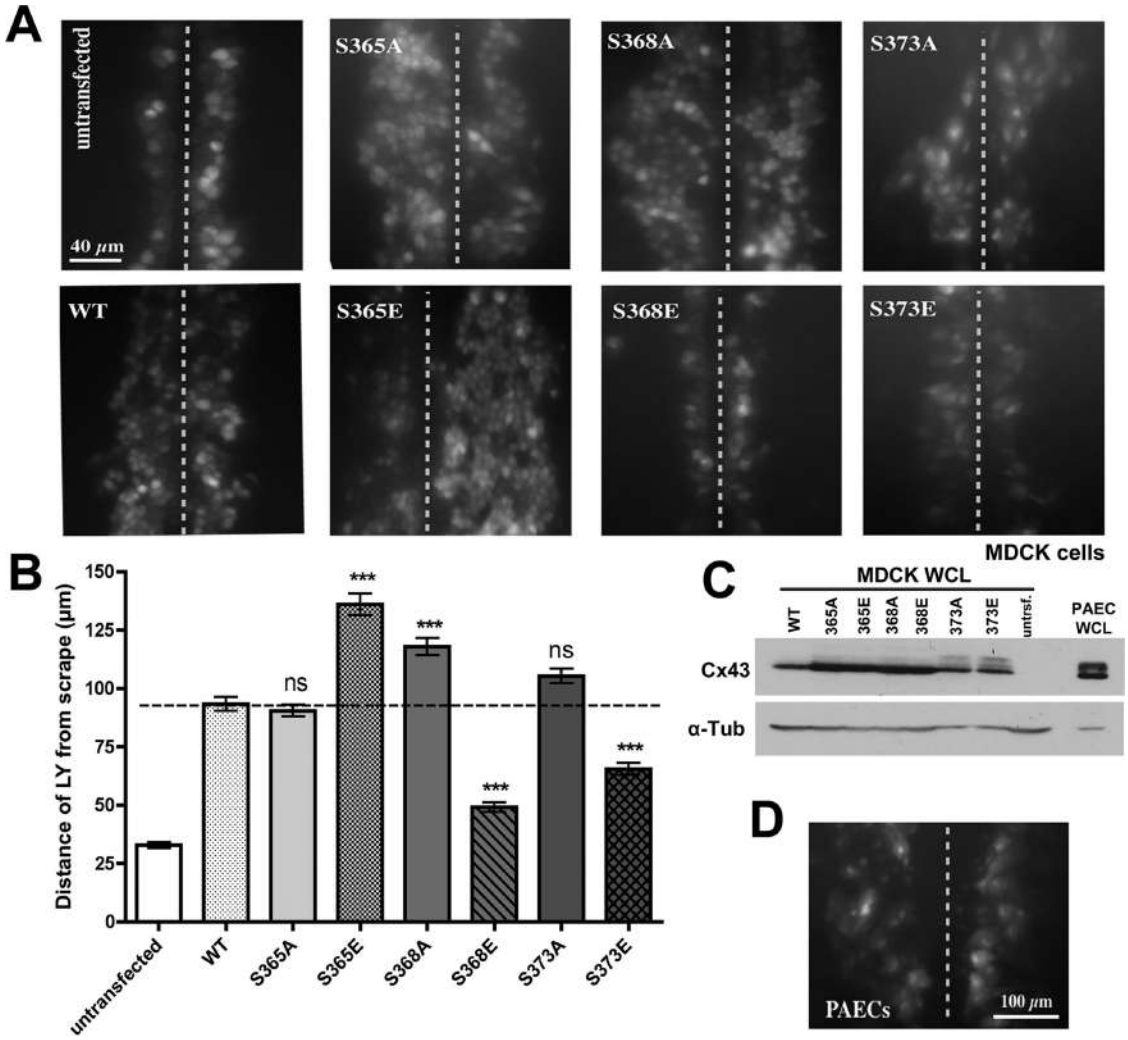

FIGURE 7: Cx43 S mutants that cannot disengage from ZO-1 stay open. (A) MDCK cells were transfected with Cx43 WT and mutant constructs. Dishes with very high transfection rates (~90%) were scraped 24 h later with a razor blade in the presence of GJ-permeable LY dye. Untransfected cells were analyzed in parallel as negative controls. After a 10-min incubation period, cells were fixed and the distance that dye spread away from the scrapes (marked with dotted lines) was measured. Representative images are shown. (B) Quantitative analyses of three independent experiments in which more than 30 images for each construct were analyzed. Asterisks mark significant differences from WT Cx43 (one-way ANOVA followed by Dunnett multiple comparison test). (C) Cx43 protein levels in cells used in the dye transfer assays were analyzed by Western blot and were found to be comparable to Cx43 protein levels found in endogenously Cx43-expressing primary PAE cells. (D) Dye transfer rates in primary PAE cells analyzed in parallel were comparable to those in transfected Cx43 WT. Note that dye transfer rates in Cx43 S365E, S368A, and S373A were significantly higher compared with Cx43 WT, suggesting that channels assembled from these mutant Cxs stayed open. WCL = whole cell lysate.

clathrin/clathrin adaptors) can access, modify, and transition Cx43 GJ channels for endocytosis.

In summary, the molecular machinery that drives accrual of newly synthesized channels to the periphery of GJ plaques and the subsequent transitioning of functional channels into nonfunctional channels (permanently closed) that then are endocytosed from central plaque areas appears complex, and is driven by a number of consecutive Cx43 phosphorylation and dephosphorylation events (Figure 8). Taking into account work by others, our results suggest that 1) S365 and S373 phosphorylation (by PKA and Akt, respectively)—probably occurring early in the secretory pathway—promote forward trafficking, potentially regulated via Akt phosphorylation of S373 and interaction with 14–3–3 protein (Park *et al.*, 2006, 2007). In addition, phosphorylation on these residues appears to prevent premature binding of ZO-1 to plasma membrane-delivered Cxs, potentially allowing them to function as hemichannels before they can dock and accrue to GJ plaques. 2) S373 dephosphorylation then permits ZO-1 to bind to Cxs, and Cxs to dock and accrue to GJ plaques. These newly accrued channels are likely to be open and functional. 3) Subsequent dephosphorylation of S365 followed by concomitant phosphorylation of S368 (by PKC) then induces release of ZO-1 from Cx43 and GJ channels to close (permanently). Continuing accrual of newly synthesized channels to plaque edges then drives aged/closed channels inward that then, triggered by additional Cx43 posttranslational modifications, namely MAPK-mediated phosphorylation and ubiquitination (Fong *et al.*, 2014; Nimlamool *et al.*, 2015; Kells-Andrews and Falk, 2017), permits clathrin recruitment and GJ channel endocytosis. Interestingly, Solan *et al.* (2007) found that a Cx43 phosphomimetic mutant of S365 (S365D) underwent a large conformational change in its

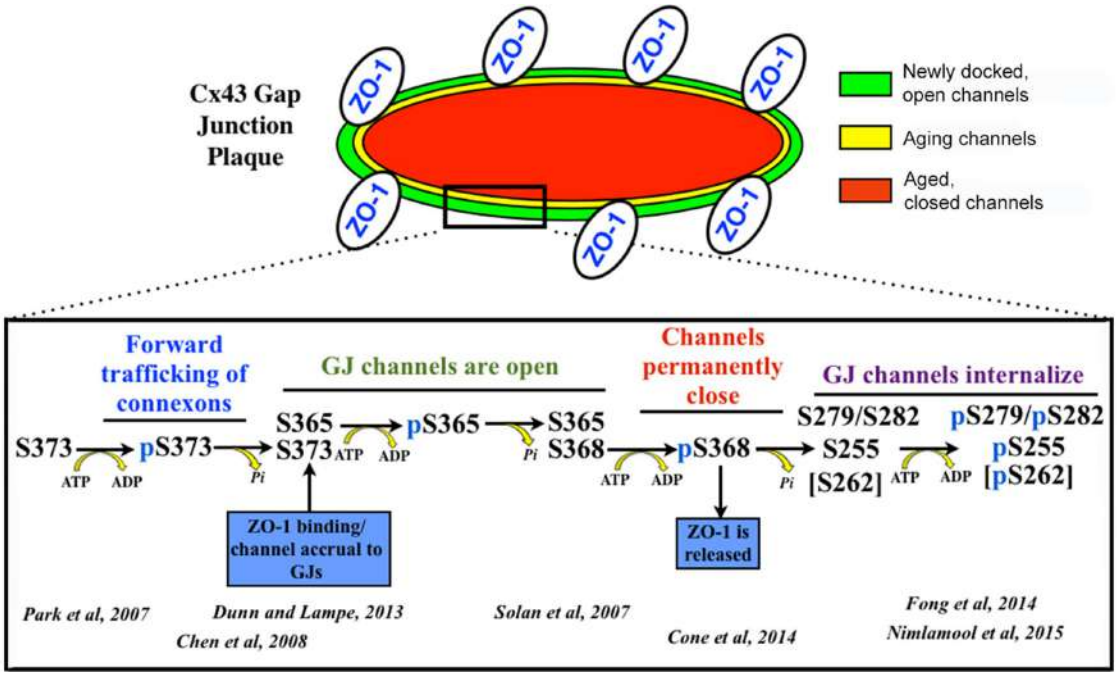

FIGURE 8: Predicted sequence of phosphorylation/dephosphorylation events indicated by our analyses and how they relate to ZO-1 binding and release, GJ channel accrual, opening and closing, and endocytosis. A scheme of a GJ plaque showing newly accrued functional channels (open) with bound ZO-1 located in the periphery (green), transitioning/aging channels (yellow), and aged, nonfunctional (closed) channels that no longer interact with ZO-1 and are primed for endocytosis in the plaque center (red) is shown. S373 is likely phosphorylated early on during the oligomerization of Cx43 into Cxs and forward trafficking towards the plasma membrane. Cx43 phosphorylated on S373 does not interact with ZO-1. Once S373 is dephosphorylated, ZO-1 can bind Cx43. S365 is phosphorylated concurrently with S373 dephosphorylation, or shortly before or after. GJ channels are open and functional. When S365 becomes dephosphorylated, S368 can be phosphorylated, causing channels to close. ZO-1 releases in response to these phosphorylation/dephosphorylation events. Earlier we reported that phosphorylation on S368, S255, S279, and S282 down-regulates GJIC (through channel closure) and causes Cx43 GJs to internalize (Fong *et al.*, 2014; Nimlamool *et al.*, 2015). This suggests that later MAPK phosphorylation events in the vicinity of the clathrin/clathrin-adaptor binding sites primes aged, nonfunctional (closed) GJ channels for endocytosis. Key works by others and us that correlate with our findings are referenced.

C-terminal domain that also included a distant, upstream-located domain that we now know harbors the Cx43 endocytic motifs (Thomas *et al.*, 2003; Fong *et al.*, 2013). It thus is possible that in newly accrued (functional) channels in which S368 has not yet become phosphorylated, access of MAP kinases, ubiquitin ligases, and clathrin/clathrin-adaptors to the Cx43-C-terminus is simply sterically blocked, while in aged channels in which S368 is phosphorylated (nonfunctional, permanently closed), access—triggered by the conformational change—is permitted (Falk *et al.*, 2016). Certainly, implementing a sequence of different regulatory modifications (binding/release of a scaffolding protein, early and late phosphorylation/dephosphorylation events, ubiquitination) instead of transitioning GJ channels from functional to nonfunctional by a single event increases specificity and flexibility, including the ability to abort and revert the chain of events in case changing cellular conditions call for a modification in GJIC and/or physical cell–cell adhesion. As the first reports now link altered, nonphysiological GJ turnover rates to disease (Berthoud *et al.*, 2013; Gemel *et al.*, 2014; reviewed in Laird, 2014; Kelly *et al.*, 2015), and Cx43 polypeptides with altered or deleted C-terminal domains exhibit impaired turnover characteristics (Maass *et al.*, 2007; Vreeburg *et al.*, 2007; Remo *et al.*, 2011), understanding the molecular machinery that drives the dynamic turnover of gap junctions appears particularly significant.

MATERIALS AND METHODS

cDNA constructs and mutagenesis

Untagged Cx43 mutants were generated by the Quick Change mutagenesis method (Stratagene) using WT rat Cx43 cDNA cloned into pEGFP-N1 vector (Clontech) as previously described (Falk, 2000). A Cx43 authentic TAA stop codon was reintroduced to allow expression of full-length untagged Cx43. Forward mutagenesis primers were as follows (mutated codons are underlined): Cx43-Stop, 5′-CCT GAT GAC CTG GAG ATT TAA GAT CCA CCG GTC GCC ACC-3′; S365A, 5′-ATC GTG GAC CAA CGA CCT TCC GCA AGA GCC AGC AGC CGC GCC AGC-3′; S365E, 5′-ATC GTG GAC CAA CGA CCT TCC GAA AGA GCC AGC AGC CGC GCC AGC-3′; S368A, 5′-CAA CGA CCT TCC AGC AGA GCC GCA AGC CGC GCC AGC AGC AGG CCT-3′; S368E, 5′-CAA CGA CCT TCC AGC AGA GCC GAA AGC CGC GCC AGC AGC AGG CCT-3′; S373A, 5′-GCC AGC AGC CGC GCC AGC GCA AGG CCT CGG CCT GAT GAC-3′; S373E, 5′-GCC AGC AGC CGC GCC AGC GAA AGG CCT CGG CCT GAT GAC-3′; S255A, 5′-CAC GCC ACC ACT GGC CCA CTG GCA CCA TCA AAA GAC TGC GGA TCT-3′; S255E, 5′-CAC GCC ACC ACT GGC CCA CTG GAA CCA TCA AAA GAC TGC GGA TCT-3′; S279A/S282A, 5′-CC TCA CCA ACG GCT CCA CTC GCA CCT ATG GCA CCT CCT GGG TAC AAG CTG G-3′; and S279E/S282E, 5′-CC TCA CCA ACG GCT CCA CTC GAA CCT ATG

GAA CCT CCT GGG TAC AAG CTG G-3′. PCR mutagenesis reactions were performed with proofreading *Pfu* Ultra II polymerase (cat. no. 600670-51; Stratagene), per Quick Change mutagenesis protocol provided by Stratagene and DNA was digested with *Dpn*I (cat. no. R0176-S; New England Biolabs) per Quick Change mutagenesis protocol provided by Stratagene and transformed into maximum-efficiency chemically competent DH5α *Escherichia coli* cells (cat. no. 18258-012; Invitrogen). All DNA constructs were sequenced to verify the presence of the intended mutations.

Cell culture and transfections

Cx-deficient HeLa cells (cat. no. CCL-2; American Type Culture Collection [ATCC]) were maintained at 37°C, 5% CO_2 in high glucose DMEM. Media were supplemented for a final concentration of 10% with fetal bovine serum (FBS), 2 mM L-glutamine, 50 IU/ml penicillin, and 50 μg/ml streptomycin. Cx-deficient MDCK cells (cat. no. CRL-2936; ATCC) (Dukes *et al.*, 2011) and primary porcine PAECs, isolated as described previously (Baker *et al.*, 2008), were maintained under the same conditions, except in low-glucose DMEM supplemented with the same additions as media used for HeLa cells. For transfection experiments, HeLa or MDCK cells were passaged 24 h prior to transfections and seeded to reach ~75% confluency. Cells were transfected with Lipofectamine2000 (cat. no. 11668027; Invitrogen) as recommended by the manufacturer. Transfection efficiencies of ~25% for HeLa and up to ~90% for MDCK cells were routinely achieved. PAECs endogenously expressing high levels of Cx43 served as a positive control.

Immunofluorescence microscopy and quantitative image analyses

Cells were grown on glass coverslips pretreated with poly-L-lysine (cat. no. P8920; Sigma-Aldrich), fixed with 3.7% formaldehyde at room temperature (RT) for 15 min, and permeabilized with 0.2% Triton X-100 in phosphate-buffered saline (PBS) at RT for 15 min. Cells were then blocked with 10% FBS in PBS at RT for 30 min and incubated with rabbit polyclonal anti-Cx43 antibodies (cat. no. 3512; Cell Signaling Technology) at 1:200 dilution at 4°C overnight. Secondary antibodies (Alexa Fluor488-conjugated goat anti-rabbit, cat. no. A11008; Molecular Probes/Invitrogen) were used at 1:1000 dilution at RT for 1 h. Cells were rinsed in PBS and blocked with 10% FBS and then incubated with mouse monoclonal anti-ZO-1 antibodies (cat. no. 339100; Invitrogen) at 1:200 dilution at 4°C overnight. Secondary antibodies (Alexa Fluor568-conjugated goat anti-mouse, cat. no. A11031; Molecular Probes) were used at 1:1000 dilution for 1 h at RT. Cell nuclei were stained with 1 μg/ml 4′,6-diamidino-2-phenylindole (DAPI). Cells were mounted using Fluoromount-G (cat. no. 0100-01; Southern Biotechnology) after coverslips were rinsed in distilled water. Slides were examined either with a Zeiss 880 confocal microscope, a Zeiss 880 confocal microscope equipped with AiryScan, or a Nikon Eclipse TE 2000E inverted fluorescence microscope, equipped with either 60×, 63×, or 100× NA 1.3 and NA 1.4 Plan-Apochromat oil-immersion objectives (Nikon Instruments; Carl Zeiss) and a Photonics CoolSnap HQ CCD camera (Roper Scientific). Images shown in Supplemental Figure S2 were acquired with a 100× objective with additional 1.5× auxiliary magnification to further boost CCD camera resolution. Wide-field images were acquired using MetaVue software version 6.1r5 (Molecular Devices). Quantitative image analyses comparing cytosolic and GJ bound ZO-1, line scan analyses, and GJ plaque area analyses were performed using ImageJ version 1.41o (National Institutes of Health; see legends of Supplemental Figures S5 and S6 for details). For line scan analyses, the "Line Scan Tool" in MetaVue software was used and data points were exported and analyzed in MS Excel. To calculate levels of cytosolic versus GJ-bound ZO-1, images were exported into ImageJ and areas of measurement were outlined and quantified. In each image, at least two areas of cytosolic ZO-1 in cells not expressing any Cx43 were compared with cytosolic levels of ZO-1 in cells that expressed Cx43 and GJ-bound ZO-1 calculated (Supplemental Figure S5). Data are averages of at least three independent experiments with at least 20 images per experiment and mutant. For GJ plaque size/number analyses, images were exported into ImageJ software and areas of cell–cell contacts containing visible Cx43 fluorescence signals were selected and quantified. Data are expressed as averages of performed experiments with at least 25–30 images per experiment and mutant.

Coimmunoprecipitation assays

HeLa or MDCK cells transfected with WT or mutant Cx43 cDNAs were trypsinized and grown for 24 h, rinsed in ice-cold PBS, and lysed in lysis buffer (1× RIPA buffer, cat. no. 9806; Cell-Signaling Technology) in the presence of protease inhibitors (cat. no. P8340; Sigma-Aldrich) and 1 mM Na_3VO_4 and 1 mM β-glycerophosphate (to block phosphatase activity) for 20 min on ice. A quantity of 10 μl of Protein-G Dynabeads (cat. no. 10003D; Invitrogen)/sample was washed in 500 μl of PBS/0.02% Tween20. For ZO-1/Cx43 coimmunoprecipitations, the beads were incubated with 1 μl of mouse monoclonal ZO-1 antibody for 1 h at RT. For clathrin heavy-chain/Cx43 coimmunoprecipitation, the beads were incubated with 1 μl of mouse monoclonal clathrin heavy-chain antibody (cat. no. 610499; BD Transduction Laboratories) for 1 h at RT. Bead/antibody mixtures were washed twice in 500 μl PBS/0.02% Tween20 and added to cell lysates, which were first centrifuged at 14,000 rpm to remove cell debris and organelles. Cleared cell lysates (typically 800 μl prepared from a 6-cm-diameter culture dish of confluent cells) were incubated with antibody/beads conjugates for 2 h at RT, washed twice in 500 μl of lysis buffer, and eluted with 30 μl of 2 × SDS–PAGE sample buffer. Beads were boiled for 5 min, and eluted proteins were analyzed by SDS–PAGE and Western blot analyses.

SDS–PAGE and Western blot analyses

Proteins were resolved on 10% SDS–PAGE gels, transferred to nitrocellulose membranes, blocked with 5% nonfat dry milk in TBS/0.1% Tween20 (TBS-T), washed three times in TBS-T, and incubated overnight in primary antibodies in 5% BSA/TBS (BSA cat. no. A7906; Sigma Aldrich) at 4°C. Antibody dilutions were as follows: rabbit Cx43 (Cell Signaling), 1:2000; mouse ZO-1 (Invitrogen), 1:1000; mouse clathrin heavy chain (BD Transduction), 1:2000; α-tubulin (cat. no. T2096, Sigma-Aldrich), 1:5000. Blots were washed three times in TBS-T and incubated in the appropriate secondary antibodies (goat anti-mouse-HRP and goat anti-rabbit HRP, cat. nos. G21040 and G21234, respectively; Invitrogen) for 30 min at 1:3000 dilution at RT. Relevant proteins were detected with enhanced chemiluminescent reagent. ImageJ (Nationl Institutes of Health) was used to quantify protein band intensities.

Triton X-100 solubility assays

Triton X-100 solubility assays were performed as described by Musil and Goodenough (1991) with the following modifications: 70–75% confluent 3.5-cm dishes of MDCK cells were transfected with WT or mutant Cx43 cDNAs using Lipofectamine2000. At 20 h posttransfection, cells were lysed for 20 min in 400 μl of prechilled lysis buffer containing 50 mM Tris-HCl, pH 7.4, 150 mM NaCl, 1 mM EDTA, 0.5% sodium deoxycholate, and 1% Triton X-100. The buffer was supplemented with protease and phosphatase inhibitors as described above. Cells were scraped off the dishes, and lysates were

transferred into 1.5 ml Eppendorf tubes and centrifuged at 10,000 × *g* for 5 min at RT to preclear cell lysates. A 180-µl sample of each resulting supernatant was centrifuged at 100,000 × *g* in a Beckman Coulter Airfuge ultracentrifuge for 8 min. Supernatant fractions were immediately removed and transferred into new tubes, while remaining pellets were resuspended in 20 µl of 2× SDS–PAGE sample buffer. For Western blot analyses, 40 µl of the soluble fraction (100,000 × *g* supernatants) were mixed with 13.3 µl of 4× SDS–PAGE sample buffer. Total fractions (10,000 × *g* supernatants) were prepared in the same manner in controls. For each construct, 15 µl of the soluble fraction and 15 µl of the total fraction were resolved by SDS–PAGE. The entire 20 µl of the insoluble fraction (100,000 × *g* pellet) was analyzed by SDS–PAGE using anti-ZO-1 antibodies. Probed membranes were then stripped and reprobed with Cx43 antibodies. Identical procedures were applied when HeLa or PAECs were analyzed.

Cx43 protein half-life analyses

A set of 70–75% confluent 3.5-cm dishes (seven per construct and experiment) were transfected either with WT or with respective mutant Cx43 cDNA using Lipofectamine2000. At 20 h posttransfection, six dishes each were treated with 50 µg/ml cycloheximide (cat. no. C6255; Sigma-Aldrich) and kept in an incubator at 37°C, 5% CO_2. One dish was designated as an untreated control; it was rinsed at RT in 1× PBS and cells were lysed with 500 µl of 1× SDS–PAGE sample buffer. At various time points (30 min and 1, 2, 3, 4, and 6 h), remaining dishes were treated as described for the control. All samples were immediately boiled for 5 min and stored at –80°C for subsequent SDS–PAGE and Western blot analyses (15 µl/sample) using Cx43 antibodies. Probed membranes were stripped and reprobed with anti α-tubulin specific antibodies to control for equal loading. Intensities of Cx43 and α-tubulin bands were analyzed using ImageJ software and Cx43 signals were normalized to the intensity of the corresponding α-tubulin signals.

Scrape-loading dye-transfer assays

MDCK cells were seeded on poly-L-lysine–coated glass coverslips placed into 3.5-cm dishes and grown to 50-75% confluence. In parallel, 3.5-cm dishes not containing coverslips were also seeded with cells. Dishes with and without coverslips were transfected with WT or mutant Cx43 cDNAs, leaving one set of dishes as untransfected controls. At 20 h posttransfection, cells (then close to confluency) in the dishes without coverslips were rinsed in 1× PBS, resuspended in 1× SDS PAGE sample buffer, boiled for 5 min, and used for Western blot analyses to detect expression levels of Cx43. Cells in the dishes containing coverslips were rinsed in 1××x PBS at RT, and 1 ml of 0.05 weight % LY (cat. no. L682; Invitrogen) in 1× PBS was added to each dish. Monolayers were scraped with a sharp razor blade and incubated at 37°C under 5% CO_2 for 10 min. Cells then were rinsed quickly in 1× PBS and fixed in 3.7% formaldehyde for 10 min at RT. Cover slips were rinsed three times in 1× PBS and dye transfer was imaged with a 20× objective on a Nikon Eclipse TE 2000E inverted fluorescence microscope. Scrape-loading dye-transfer assays were also performed with PAECs as a positive control, as described previously (Baker *et al.*, 2008). A comparable sample of whole-cell lysate derived from PAECs was analyzed in controls to compare Cx43 expression levels in MDCK cells with the expression level in endogenously Cx43-expressing cells.

Statistical analyses

All error bars were calculated as ±SEM in GraphPad Prism (version 4.0 for Macintosh) (GraphPad, La Jolla, CA). To calculate statistical significance, ordinary one-way ANOVAs were performed, followed with Dunnett multiple comparison tests (as compared with the WT), with 95% confidence ($p \leq 0.05$). Asterisks represent statistically significant differences, where $*p < 0.05$, $**p < 0.005$, and $***p < 0.0005$.

ACKNOWLEDGMENTS

We thank Tanay Desai and Renee Dalrymple at Carl Zeiss Microscopy Labs for their help with AiryScan superresolution confocal microscopy, Lynne Cassimeris for letting us use instrumentation critical for the execution of Triton X-100 solubility studies, and current and previous Falk lab members for constructive discussions and critical reading of the manuscript. This work was supported by the National Institute of Health's National Institute of General Medical Sciences Grant GM55725 to M.M.F and funds from Lehigh University.

REFERENCES

Baker SM, Kim N, Gumpert AM, Segretain D, Falk MM (2008). Acute internalization of gap junctions in vascular endothelial cells in response to inflammatory mediator-induced G-protein coupled receptor activation. FEBS Lett 582, 4039–4046.

Beardslee MA, Laing JG, Beyer EC, Saffitz JE (1998). Rapid turnover of connexin43 in the adult rat heart. Circ Res 83, 629–635.

Berthoud VM, Minogue PJ, Laing JG, Beyer EC (2004). Pathways for degradation of connexins and gap junctions. Cardiovasc Res 62, 256–267.

Berthoud VM, Minogue PJ, Yu H, Schroeder R, Snabb JI, Beyer EC (2013). Connexin50D47A decreases levels of fiber cell connexins and impairs lens fiber cell differentiation. Invest Ophthalmol Vis Sci 54, 7614–7622.

Boassa D, Solan JL, Papas A, Thornton P, Lampe PD, Sosinsky GE (2010). Trafficking and recycling of the connexin43 gap junction protein during mitosis. Traffic 11, 1471–1486.

Bruzzone R, White TW, Paul DL (1996). Connections with connexins: the molecular basis of direct intercellular signaling. Eur J Biochem 238, 1–27.

Bukauskas FF, Jordan K, Bukauskiene A, Bennett MV, Lampe PD, Laird DW, Verselis VK (2000). Clustering of connexin 43-enhanced green fluorescent protein gap junction channels and functional coupling in living cells. Proc Natl Acad Sci USA 97, 2556–2561.

Chen HI, Sudol M (1995). The WW domain of Yes-associated protein binds a proline-rich ligand that differs from the consensus established for Src homology 3-binding modules. Proc Natl Acad Sci USA 92, 7819–7823.

Chen J, Pan L, Wei Z, Zhao Y, Zhang M (2008). Domain-swapped dimerization of ZO-1 PDZ2 generates specific and regulatory connexin43-binding sites. EMBO J 27, 2113–2123.

Cone AC, Gavin G, Ambrosi C, Hakozaki H, Wu-Zhang AX, Kunkel MT, Newton AC, Sosinsky GE (2014). Protein kinase Cδ-mediated phosphorylation of Connexin43 gap junction channels causes movement within gap junctions followed by vesicle internalization and protein degradation. J Biol Chem 289, 8781–8798.

Curti S, Hoge G, Nagy JI, Pereda AE (2012). Synergy between electrical coupling and membrane properties promotes strong synchronization of neurons of the mesencephalic trigeminal nucleus. J Neurosci 32, 4341–4359.

Dukes JD, Whitley P, Chalmers AD (2011). The MDCK variety pack: choosing the right strain. BMC Cell Biol 12, 43.

Dunn CA, Lampe PD (2014). Injury-triggered Akt phosphorylation of Cx43: a ZO-1-driven molecular switch that regulates gap junction size. J Cell Sci 127, 455–464.

Falk MM (2000). Connexin-specific distribution within gap junctions revealed in living cells. J Cell Sci 113(Pt 22), 4109–4120.

Falk MM, Baker SM, Gumpert AM, Segretain D, Buckheit RW 3rd (2009). Gap junction turnover is achieved by the internalization of small endocytic double-membrane vesicles. Mol Biol Cell 20, 3342–3352.

Falk MM, Bell CL, Kells Andrews RK, Murray SA (2016). Molecular mechanisms regulating formation, trafficking and processing of annular gap junctions. BMC Cell Biol 17 (Suppl 1), 22.

Falk MM, Kells RM, Berthoud VM (2014). Degradation of connexins and gap junctions. FEBS Lett 588, 1221–1229.

Fallon RF, Goodenough DA (1981). Five-hour half-life of mouse liver gap-junction protein. J Cell Biol 90, 521–526.

Flores CE, Nannapaneni S, Davidson KG, Yasumura T, Bennett MV, Rash JE, Pereda AE (2012). Trafficking of gap junction channels at a vertebrate electrical synapse in vivo. Proc Natl Acad Sci USA 109, E573–E582.

Fong JT, Kells RM, Falk MM (2013). Two tyrosine-based sorting signals in the Cx43 C-terminus cooperate to mediate gap junction endocytosis. Mol Biol Cell 24, 2834–2848.

Fong JT, Nimlamool W, Falk MM (2014). EGF induces efficient Cx43 gap junction endocytosis in mouse embryonic stem cell colonies via phosphorylation of Ser262, Ser279/282, and Ser368. FEBS Lett 588, 836–844.
Gaietta G, Deerinck TJ, Adams SR, Bouwer J, Tour O, Laird DW, Sosinsky GE, Tsien RY, Ellisman MH (2002). Multicolor and electron microscopic imaging of connexin trafficking. Science 296, 503–507.
Gemel J, Simon AR, Patel D, Xu Q, Matiukas A, Veenstra RD, Beyer EC (2014). Degradation of a connexin40 mutant linked to atrial fibrillation is accelerated. J Mol Cell Cardiol 74, 330–339.
Giepmans BN (2006). Role of connexin43-interacting proteins at gap junctions. Adv Cardiol 42, 41–56.
Giepmans BN, Moolenaar WH (1998). The gap junction protein connexin43 interacts with the second PDZ domain of the zona occludens-1 protein. Curr Biol 8, 931–934.
Gilleron J, Carette D, Fiorini C, Dompierre J, Macia E, Denizot JP, Segretain D, Pointis G (2011). The large GTPase dynamin2: a new player in connexin 43 gap junction endocytosis, recycling and degradation. Int J Biochem Cell Biol 43, 1208–1217.
Gilleron J, Fiorini C, Carette D, Avondet C, Falk MM, Segretain D, Pointis G (2008). Molecular reorganization of Cx43, Zo-1 and Src complexes during the endocytosis of gap junction plaques in response to a non-genomic carcinogen. J Cell Sci 121, 4069–4078.
Ginzberg RD, Gilula NB (1979). Modulation of cell junctions during differentiation of the chicken otocyst sensory epithelium. Dev Biol 68, 110–129.
Gumpert AM, Varco JS, Baker SM, Piehl M, Falk MM (2008). Double-membrane gap junction internalization requires the clathrin-mediated endocytic machinery. FEBS Lett 582, 2887–2892.
Herve JC, Derangeon M, Sarrouilhe D, Giepmans BN, Bourmeyster N (2012). Gap junctional channels are parts of multiprotein complexes. Biochim Biophys Acta 1818, 1844–1865.
Hesketh GG, Shah MH, Halperin VL, Cooke CA, Akar FG, Yen TE, Kass DA, Machamer CE, Van Eyk JE, Tomaselli GF (2010). Ultrastructure and regulation of lateralized connexin43 in the failing heart. Circ Res 106, 1153–1163.
Hunter AW, Barker RJ, Zhu C, Gourdie RG (2005). Zonula occludens-1 alters connexin43 gap junction size and organization by influencing channel accretion. Mol Biol Cell 16, 5686–5698.
Hunter AW, Jourdan J, Gourdie RG (2003). Fusion of GFP to the carboxyl terminus of connexin43 increases gap junction size in HeLa cells. Cell Commun Adhes 10, 211–214.
Johnson KE, Mitra S, Katoch P, Kelsey LS, Johnson KR, Mehta PP (2013). Phosphorylation on serines 279 and 282 of Connexin43 regulates endocytosis and gap junction assembly in pancreatic cancer cells. Mol Biol Cell 24, 715–733.
Johnstone SR, Billaud M, Lohman AW, Taddeo EP, Isakson BE (2012). Post-translational modifications in connexins and pannexins. J Membr Biol 245, 319–332.
Kells-Andrews RM, Falk MM (2017). Phosphorylation-induced K63-polyubiquitination of connexin 43 regulates gap junction internalization. bioRxiv, doi: https://doi.org/10.1101/211607.
Kelly JJ, Simek J, Laird DW (2015). Mechanisms linking connexin mutations to human diseases. Cell Tissue Res 360, 701–721.
Kretz M, Euwens C, Hombach S, Eckardt D, Teubner B, Traub O, Willecke K, Ott T (2003). Altered connexin expression and wound healing in the epidermis of connexin-deficient mice. J Cell Sci 116, 3443–3452.
Kumar NM, Gilula NB (1996). The gap junction communication channel. Cell 84, 381–388.
Laird DW (2014). Syndromic and non-syndromic disease-linked Cx43 mutations. FEBS Lett 588, 1339–1348.
Lambiase PD, Tinker A (2015). Connexins in the heart. Cell Tissue Res 360, 675–684.
Lauf U, Giepmans BN, Lopez P, Braconnot S, Chen SC, Falk MM (2002). Dynamic trafficking and delivery of connexons to the plasma membrane and accretion to gap junctions in living cells. Proc Natl Acad Sci USA 99, 10446–10451.
Leach DH, Oliphant LW (1984). Degradation of annular gap junctions of the equine hoof wall. Acta Anat (Basel) 120, 214–219.
Lin J, Li Y, Lin S, Liang Q, Tan X (2007). The effect of delayed preconditioning on connexin 43 in ischemic myocardium. Biochem Cell Biol 85, 175–181.
Lo CW, Gilula NB (1979). Gap junctional communication in the preimplantation mouse embryo. Cell 18, 399–409.
Maass K, Shibayama J, Chase SE, Willecke K, Delmar M (2007). C-terminal truncation of connexin43 changes number, size, and localization of cardiac gap junction plaques. Circ Res 101, 1283–1291.
Meens MJ, Kwak BR, Duffy HS (2015). Role of connexins and pannexins in cardiovascular physiology. Cell Mol Life Sci 72, 2779–2792.
Musil LS, Goodenough DA (1991). Biochemical analysis of connexin43 intracellular transport, phosphorylation, and assembly into gap junctional plaques. J Cell Biol 115, 1357–1374.
Nakano Y, Oyamada M, Dai P, Nakagami T, Kinoshita S, Takamatsu T (2008). Connexin43 knockdown accelerates wound healing but inhibits mesenchymal transition after corneal endothelial injury in vivo. Invest Ophthalmol Vis Sci 49, 93–104.
Nickel B, Boller M, Schneider K, Shakespeare T, Gay V, Murray SA (2013). Visualizing the effect of dynamin inhibition on annular gap vesicle formation and fission. J Cell Sci 126, 2607–2616.
Nimlamool W, Kells Andrews RM, Falk MM (2015). Connexin43 phosphorylation by PKC and MAPK signals VEGF-mediated gap junction internalization. Mol Biol Cell, 26, 2755–2768.
Nlend RN, Michon L, Bavamian S, Boucard N, Caille D, Cancela J, Charollais A, Charpantier E, Klee P, Peyrou M, *et al*. (2006). Connexin36 and pancreatic beta-cell functions. Arch Physiol Biochem 112, 74–81.
Park DJ, Freitas TA, Wallick CJ, Guyette CV, Warn-Cramer BJ (2006). Molecular dynamics and in vitro analysis of Connexin43: a new 14-3-3 mode-1 interacting protein. Protein Sci 15, 2344–2355.
Park DJ, Wallick CJ, Martyn KD, Lau AF, Jin C, Warn-Cramer BJ (2007). Akt phosphorylates Connexin43 on Ser373, a "mode-1" binding site for 14-3-3. Cell Commun Adhes 14, 211–226.
Piehl M, Lehmann C, Gumpert A, Denizot JP, Segretain D, Falk MM (2007). Internalization of large double-membrane intercellular vesicles by a clathrin-dependent endocytic process. Mol Biol Cell 18, 337–347.
Qiu C, Coutinho P, Frank S, Franke S, Law LY, Martin P, Green CR, Becker DL (2003). Targeting connexin43 expression accelerates the rate of wound repair. Curr Biol 13, 1697–1703.
Remo BF, Giovannone S, Fishman GI (2012). Connexin43 cardiac gap junction remodeling: lessons from genetically engineered murine models. J Membr Biol 245, 275–281.
Remo BF, Qu J, Volpicelli FM, Giovannone S, Shin D, Lader J, Liu FY, Zhang J, Lent DS, Morley GE, Fishman GI (2011). Phosphatase-resistant gap junctions inhibit pathological remodeling and prevent arrhythmias. Circ Res 108, 1459–1466.
Rhett JM, Jourdan J, Gourdie RG (2011). Connexin 43 connexon to gap junction transition is regulated by zonula occludens-1. Mol Biol Cell 22, 1516–1528.
Solan JL, Lampe PD (2005). Connexin phosphorylation as a regulatory event linked to gap junction channel assembly. Biochim Biophys Acta 1711, 154–163.
Solan JL, Lampe PD (2007). Phosphorylation at S365 is a gatekeeper event that changes the structure of Cx43 and prevents down-regulation by PKC. J Cell Biol 179, 1301–1309.
Solan JL, Lampe PD (2009). Connexin43 phosphorylation: structural changes and biological effects. Biochem J 419, 261–272.
Solan JL, Lampe PD (2014). Specific Cx43 phosphorylation events regulate gap junction turnover in vivo. FEBS Lett 588, 1423–1429.
Solan JL, Lampe PD (2016). Kinase programs spatiotemporally regulate gap junction assembly and disassembly: effects on wound repair. Semin Cell Dev Biol 50, 40–48.
Solan JL, Marquez-Rosado L, Sorgen PL, Thornton PJ, Gafken PR, Lampe PD (2007). Phosphorylation at S365 is a gatekeeper event that changes the structure of Cx43 and prevents down-regulation by PKC. J Cell Biol 179, 1301–1309.
Spagnol G, Kieken F, Kopanic JL, Li H, Zach S, Stauch KL, Grosely R, Sorgen PL (2016). Structural studies of the Nedd4 WW domains and their selectivity for the Connexin43 (Cx43) carboxyl terminus. J Biol Chem 291, 7637–7650.
Thevenin AF, Kowal TJ, Fong JT, Kells RM, Fisher CG, Falk MM (2013). Proteins and mechanisms regulating gap-junction assembly, internalization, and degradation. Physiology (Bethesda) 28, 93–116.
Thomas MA, Zosso N, Scerri I, Demaurex N, Chanson M, Staub O (2003). A tyrosine-based sorting signal is involved in connexin43 stability and gap junction turnover. J Cell Sci 116, 2213–2222.
Toyofuku T, Yabuki M, Otsu K, Kuzuya T, Hori M, Tada M (1998). Direct association of the gap junction protein connexin-43 with ZO-1 in cardiac myocytes. J Biol Chem 273, 12725–12731.
Vreeburg M, de Zwart-Storm EA, Schouten MI, Nellen RG, Marcus-Soekarman D, Devies M, van Geel M, van Steensel MA (2007). Skin changes in oculo-dento-digital dysplasia are correlated with C-terminal truncations of connexin 43. Am J Med Genet A 143, 360–363.
Wang CM, Lincoln J, Cook JE, Becker DL (2007). Abnormal connexin expression underlies delayed wound healing in diabetic skin. Diabetes 56, 2809–2817.